www.elsevier.nl/locate/jorganchem

Journal of Organometallic Chemistry 593–594 (2000) 325–334

Journal of Organometallic Chemistry

Synthesis and characterization of new paramagnetic nickel carbonyl clusters containing antimony atoms: X-ray structure of $[NEt_3CH_2Ph]_2[Ni_{15}(\mu_{12}\text{-}Sb)(CO)_{24}]$ and $[NEt_4]_3[Ni_{10}Sb_2(\mu_{12}\text{-}Ni)(CO)_{18}]$

Vincenzo G. Albano [a,*], Francesco Demartin [b], Cristina Femoni [c], Maria Carmela Iapalucci [c], Giuliano Longoni [c,1], Magda Monari [a], Piero Zanello [d]

[a] *Dipartimento di Chimica 'G. Ciamician', Università di Bologna, via F. Selmi 2, I-40126 Bologna, Italy*
[b] *Dipartimento di Chimica Strutturale e Stereochimica Inorganica, Università di Milano, via G. Venezian 21, I-20133 Milan, Italy*
[c] *Dipartimento di Chimica Fisica ed Inorganica, Università di Bologna, viale del Risorgimento 4, I-40136 Bologna, Italy*
[d] *Dipartimento di Chimica, Universitò di Siena, Pian dei Mantellini 44, I-53100 Siena, Italy*

Received 16 June 1999; accepted 7 September 1999

Dedicated to Professor Fausto Calderazzo on the occasion of his 70th birthday in recognition of his outstanding contributions to chemistry.

Abstract

The reaction of the $[Ni_6(CO)_{12}]^{2-}$ dianion with $SbCl_3$ in a 2.5:1 molar ratio leads to formation of the new $[Ni_{15}(\mu_{12}\text{-}Sb)(CO)_{24}]^{2-}$, $\mathbf{1}^{2-}$, cluster with good selectivity. This has been conveniently separated from $[Ni_9(CO)_{18}]^{2-}$, $[Ni_{10}(SbNi(CO)_3)_2(\mu_{12}\text{-}Ni)(CO)_{18}]^{n-}$, $\mathbf{2}^{n-}$, $(n = 2, 3)$ and other side-products by differential solubility of their $[NEt_4]^+$ salts and isolated in 50–60% yields. The corresponding $[NEt_3CH_2Ph]_2$[**1**] salt was obtained from $[NEt_4]_2$[**1**] by metathesis in acetonitrile with $[NEt_3CH_2Ph]Cl$ and has been structurally characterized. The structure of $\mathbf{1}^{2-}$ consists of a distorted Sb-centered $Ni_{12}(\mu_{12}\text{-}Sb)$ icosahedral moiety, capped by three Ni atoms on three adjacent triangular faces. The $\mathbf{1}^{2-}$ dianion is moderately stable to oxidation and has been electrochemically reduced to the corresponding tri-, tetra- and penta-anion; these electrogenerated species are stable only on the timescale of cyclic voltammetry. The $\mathbf{1}^{2-}$ dianion is readily degraded upon exposure to an atmosphere of carbon monoxide to a mixture of $Ni(CO)_4$ and a yet uncharacterized red–violet intermediate, which has been tentatively formulated as the $[Ni_6Sb(CO)_x]^{2-}$ dianion on the basis of its spectroscopic features. The above mixture converts under nitrogen into the known $\mathbf{2}^{n-}$ $(n = 3, 4)$, through the intermediate formation of the new $[Ni_{10}Sb_2(\mu_{12}\text{-}Ni)(CO)_{18}]^{n-}$, $\mathbf{3}^{n-}$, $(n = 3, 4)$ species. Pure $\mathbf{3}^{3-}$ has been obtained by degradation of $\mathbf{2}^{3-}$ with two equivalents of triphenylphosphine by elimination of two equivalents of $Ni(CO)_3(PPh_3)$ and has been structurally characterized in its tetraethylammonium salt. The Ni-centered icosahedral $\mathbf{3}^{3-}$ trianion shows a chemical and electrochemical redox propensity comparable to that of the parent $\mathbf{2}^{3-}$ compound and is readily transformed in its corresponding $\mathbf{3}^{2-}$ and $\mathbf{3}^{4-}$ anions upon oxidation and reduction, respectively. Systematic observation of apparently exceptional electron counts and redox propensity by the above Ni-centered icosahedral clusters validate the previous attribution of these properties to the presence of interstitial nickel atoms and concomitant stabilization imparted by the peripheral antimony heteroatoms.

Keywords: Carbonyl nickel cluster; Antimony; Crystal structure; Electrochemistry

1. Introduction

A wide series of icosahedral nickel carbonyl clusters containing Group 14–16 elements has been synthesized [1–11]. As pictorially shown in Scheme 1, those displaying C_5 symmetry can be divided in four sets: (a) non-centered $[Ni_{10}(ER)_2(CO)_{18}]^{2-}$ (E = P, As, Sb, Bi; R = alkyl or aryl substituent) [1–5], (b) E-centered $[Ni_{12}(\mu_{12}\text{-}E)(CO)_{22}]^{2-}$ (E = Ge, Sn) [8], (c) Ni-centered $[Ni_{10}E_2(\mu_{12}\text{-}Ni)(CO)_{18}]^{n-}$ (E = Se, Bi; $n = 2$–4) [6,11], and (d) Ni-centered $[Ni_{10}(ER)_2(\mu_{12}\text{-}Ni)(CO)_{18}]^{n-}$ (E =

* Corresponding author.
[1] Also corresponding author.

0022-328X/00/$ - see front matter
PII: S0022-328X(99)00523-9

Sn, R = alkyl substituent, $n = 2$ [7], E = Sb, R = $Ni(CO)_3$, $n = 2–4$ [9,10]). The non-centered (a) and E-centered (b) nickel clusters display conventional electron counts (viz. 13 skeletal electron pairs [11]) and do not exhibit redox propensity. In contrast, the Ni-centered species belonging to categories (c) and (d) display an apparently anomalous number of SEP (viz. 17–18). Moreover, they display electrochemically-reversible redox aptitude [6,7,9,10,12]; for instance, both $[Ni_{10}Bi_2(\mu_{12}\text{-}Ni)(CO)_{18}]^{n-}$ and $[Ni_{10}(SbNi(CO)_3)_2(\mu_{12}\text{-}Ni)(CO)_{18}]^{n-}$ are stable in at least three different oxidation states. Homoleptic carbonyl metal clusters rarely display redox propensity [13–16]. EHMO analysis of several $Ni_{10}E_2(\mu_{12}\text{-}M)(CO)_{18}$ model compounds pointed out that the out-of-phase combinations of the d orbitals of the interstitial atom with those of the icosahedral $Ni_{10}E_2$ cage are sufficiently low in energy to be populated by electrons when M = Ni [10]. This rationalized the apparently exceptional electron count of the Ni-centered clusters. Furthermore, it suggested that the presence of an interstitial nickel atom and concomitant stabilization of the metal core by the peripheral main-group elements could induce electron-sink behavior also in carbonyl clusters [17].

To further strengthen this conclusion, it appeared useful to experimentally prove that a related Sb-centered icosahedral $[Ni_{12}(\mu_{12}\text{-}Sb)(CO)_{22}]^-$ cluster would have been isoelectronic with $[Ni_{12}(\mu_{12}\text{-}E)(CO)_{22}]^{2-}$ (E = Ge, Sn) [8] and reluctant to display redox propensity. The stabilization of such a species seemed possible in view of the similar size of the Sn and Sb atoms.

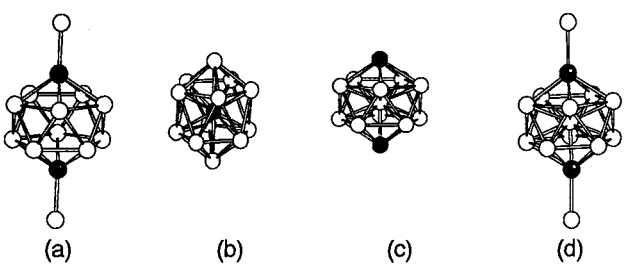

Scheme 1. Nickel and E atoms are shown as open and filled circles, respectively. Dangling circles represent alkyl, aryl or $Ni(CO)_3$ moieties.

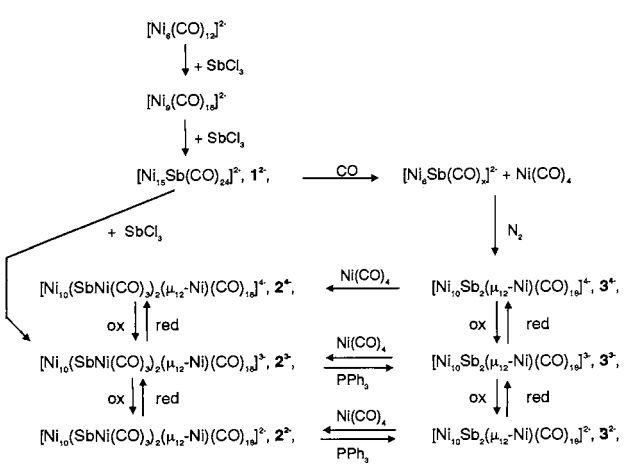

Scheme 2.

So far we only succeeded in obtaining an Sb-centered $[Ni_{15}(\mu_{12}\text{-}Sb)(CO)_{24}]^{2-}$, $\mathbf{1}^{2-}$, paramagnetic cluster, which is strictly related to the above target compound. Furthermore, the study of its chemical behavior led to isolation of the new Ni-centered $[Ni_{10}Sb_2(\mu_{12}\text{-}Ni)(CO)_{18}]^{n-}$, $\mathbf{3}^{n-}$, $(n = 2–4)$ icosahedral clusters, which may be considered as the free distibine ligand previously found in their adducts with $Ni(CO)_3$ fragments, viz. the $[Ni_{10}(SbNi(CO)_3)_2(\mu_{12}\text{-}Ni)(CO)_{18}]^{n-}$, $\mathbf{2}^{n-}$, anions [9,10].

2. Results and discussion

2.1. Synthesis and chemical characterization of $[Ni_{15}(\mu_{12}\text{-}Sb)(CO)_{24}]^{2-}$, $\mathbf{1}^{2-}$, and $[Ni_{10}Sb_2(\mu_{12}\text{-}Ni)(CO)_{18}]^{n-}$, $\mathbf{3}^{n-}$, $(n = 2, 3, 4)$

It has been reported that the reaction of $[Ni_6(CO)_{12}]^{2-}$ with $SbCl_3$ in a 1:0.7 molar ratio leads to the formation of $\mathbf{2}^{n-}$ $(n = 2, 3)$ in mixture with an uncharacterized species. Since exposure of the reaction mixture to a carbon monoxide atmosphere for short periods had beneficial effects on the yields of $\mathbf{2}^{n-}$ $(n = 2, 3)$, it was thought that the unknown species might be a higher nuclearity cluster. This was tentatively formulated as $[Ni_{23}Sb_2(CO)_x]^{4-}$ [10]. A re-investigation of the above reaction has shown that the previously unknown species actually was the quasi-icosahedral $\mathbf{1}^{2-}$ paramagnetic dianion. The study of the reactivity of $\mathbf{1}^{2-}$ toward carbon monoxide led to a better understanding of the synthesis of the $\mathbf{2}^{n-}$ cluster. Our present knowledge of the Ni–Sb carbonyl cluster system is summarized in Scheme 2.

As shown by IR monitoring, the first addition of 0.20–0.25 mol of $SbCl_3$ per mol of $[Ni_6(CO)_{12}]^{2-}$ only gives rise to oxidation of the latter to $[Ni_9(CO)_{18}]^{2-}$. A further addition of ca. 0.20 mol of $SbCl_3$ to the reaction solution results in the almost complete disappearance of $[Ni_9(CO)_{18}]^{2-}$ and formation of $\mathbf{1}^{2-}$, according to formal stoichiometry (1).

$$5[Ni_6(CO)_{12}]^{2-} + 2SbCl_3 \rightarrow 2[Ni_{15}Sb(CO)_{24}]^{2-} + 12CO + 6Cl^- \quad (1)$$

The selectivity of reaction (1) is maximized by adding very slowly the $SbCl_3$ solution and avoiding the building up of a CO partial pressure with a slow stream of nitrogen. Under these conditions, the only significant impurities are represented by $[Ni_9(CO)_{18}]^{2-}$ and $\mathbf{2}^{2-}$. The purification of $\mathbf{1}^{2-}$ is greatly favored by using $[NEt_4]_2[Ni_6(CO)_{12}]$ as starting material because of the

differential solubility of $[NEt_4]_2$[**1**] with respect to the corresponding salts of the $[Ni_9(CO)_{18}]^{2-}$ and $\mathbf{2}^{n-}$ side-products. As a result, $[NEt_4]_2$[**1**] can be advantageously purified by sequential extraction in THF and methanol of the $[Ni_9(CO)_{18}]^{2-}$ and $\mathbf{2}^{n-}$ salts. Extraction of the residue in acetone and precipitation with isopropyl alcohol affords $[NEt_4]_2$[**1**] as black crystals. Several other tetrasubstituted ammonium or phosphonium salts have been prepared by metathesis in acetonitrile and water of $[NEt_4]_2$[**1**] with their corresponding halides. Of these only the triethylbenzylammonium salt could be used in the X-ray analysis, owing to the poor diffraction properties of all other salts.

The $\mathbf{1}^{2-}$ salts show IR carbonyl absorptions at 2044 vw, 2010 s, 1970 sh, 1845 ms, and 1815 sh cm^{-1} in acetone and 2045 vw, 2006 s, 1970 sh, 1843 ms, 1810 sh cm^{-1} in acetonitrile. Acetone and acetonitrile solutions are both EPR silent in the 173–298 K temperature range. However, polycrystalline samples of the $[NEt_4]^+$ and $[NEt_3CH_2Ph]^+$ salts show an extremely broad EPR signal at $g = 2.16$ and display a magnetic moment of 1.81 BM, in keeping with the presence of an unpaired electron in the $\mathbf{1}^{2-}$ cluster ion.

The $\mathbf{1}^{2-}$ salts are moderately stable to oxidation by air. However, their reaction with $SbCl_3$ gives mainly rise to the previously reported $\mathbf{2}^{n-}$ ($n = 2$, 3), a sparingly-soluble yet unknown species (ν_{CO} in acetonitrile at 2000 s and 1845 m cm^{-1}) and some metal. As shown by independent experiments carried out on pure compounds, the yet unknown species originates directly from $\mathbf{1}^{2-}$ and not from subsequent reaction of $\mathbf{2}^{2-}$ with $SbCl_3$. Therefore, its additional formation concurs in lowering the yields of the direct synthesis of $\mathbf{2}^{n-}$ ($n = 2$, 3) [9,10]. Treatment of $\mathbf{1}^{2-}$ with oxidizing agents such as protic acids and tropylium tetrafluoroborate results in decomposition to ill-defined materials and some $\mathbf{2}^{n-}$. Its reduction with sodium naphthalenide in DMF gives likewise rise to ill-defined carbonyl species, which do not regenerate the starting material upon oxidation.

As shown in Scheme 2, the reaction of $\mathbf{1}^{2-}$ with carbon monoxide at atmospheric pressure leads to a new red–violet paramagnetic species (ν_{CO} in acetonitrile at 1965 s, 1935 m, 1770 w, and 1755w cm^{-1}; $g = 2.37$ as powder). All attempts to isolate and structurally characterize this species have so far been hampered by its extreme reactivity. First of all, this species is very sensitive to oxidation by trace amounts of air or humidity. Secondly, it is very labile under nitrogen and stable only under a carbon monoxide atmosphere in dry conditions. Thus, upon changing the atmosphere from carbon monoxide to nitrogen, the color of the solution rapidly turns brown. IR monitoring shows the formation of the new $[Ni_{10}Sb_2(\mu_{12}\text{-}Ni)(CO)_{18}]^{4-}$, $\mathbf{3}^{4-}$, and the known $\mathbf{2}^{4-}$ clusters. The latter is predominant when little effort is made to eliminate the $Ni(CO)_4$ produced along with the red–violet derivative upon degradation with CO of $\mathbf{1}^{2-}$. However, some $\mathbf{2}^{4-}$ is also obtained when $Ni(CO)_4$ is effectively removed with a stream of carbon monoxide and the resulting solution is exposed to nitrogen. In view of its chemical and spectroscopic behavior (for instance, its IR carbonyl absorptions are in keeping with a ratio between the number of metal atoms and free negative charge of ca. 3), a tentative formulation of the labile red–violet intermediate as $[Ni_6Sb(CO)_x]^{2-}$ seems reasonable. Such a species could conceivably condense into a mixture of $\mathbf{3}^{4-}$ and $\mathbf{2}^{4-}$ upon loss of carbon monoxide.

Beyond other considerations, the chemistry shown in the right side of Scheme 2 rationalizes the previously reported observation that exposure to carbon monoxide of the mixture obtained by reacting $[Ni_6(CO)_{12}]^{2-}$ and $SbCl_3$ in a ca. 0.7 molar ratio had a beneficial effect on the yields of $\mathbf{2}^{n-}$ [10]. Following this route there are no losses in side-products, as in the direct synthesis.

The above mixture of $\mathbf{2}^{n-}$ and $\mathbf{3}^{n-}$ could not be separated owing to too similar solubility of their salts both for $n = 4$ and 3. However, the new $\mathbf{3}^{3-}$ cluster has been quantitatively obtained by reacting $\mathbf{2}^{3-}$ in acetone or acetonitrile with two equivalents of triphenylphosphine, according to reaction (2).

$$\mathbf{2}^{3-} + 2PPh_3 \rightarrow \mathbf{3}^{3-} + 2Ni(CO)_3(PPh_3) \quad (2)$$

The resulting reaction mixture has been evaporated to dryness under vacuum, and washed with several portions of toluene and THF to eliminate $Ni(CO)_3(PPh_3)$. Extraction of the residue in acetone and precipitation with isopropyl alcohol affords black crystals of $[NEt_4]_3$[**3**] in high yields (80–90%). The $\mathbf{3}^{3-}$ salts show IR carbonyl absorptions at 1975 s and 1807 ms cm^{-1} in acetone and 1972 s, 1805 ms cm^{-1} in acetonitrile. Both the acetone and acetonitrile solutions are EPR silent in the 180–298 K temperature range. However, polycrystalline samples of the $[NEt_4]^+$ salt show an extremely broad EPR signal at $g = 2.023$ and display a magnetic moment of 1.86 BM after correction for diamagnetic contributions.

In keeping with the chemical behavior of the previously reported $\mathbf{2}^{3-}$ and $[Ni_{10}Bi_2(\mu_{12}\text{-}Ni)(CO)_{18}]^{3-}$ salts [10,11], $\mathbf{3}^{3-}$ is reversibly reduced by an equivalent of sodium naphthalenide in DMF to the corresponding $\mathbf{3}^{4-}$ tetraanion (ν_{CO} in DMF at 1941 s and 1790 ms cm^{-1}). Oxidation to the $\mathbf{3}^{2-}$ dianion (ν_{CO} in acetone at 1998 s and 1845 ms cm^{-1}) can be carried out with $SbCl_3$ or tropylium tetrafluoroborate. As shown by IR monitoring, the $\mathbf{3}^{4-}$ and $\mathbf{3}^{2-}$ species are stable under inert conditions for several days.

As expected, the $\mathbf{3}^{n-}$ ($n = 2$–4) cluster readily reacts with $Ni(CO)_4$ to give the corresponding $\mathbf{2}^{n-}$ ($n = 2$–4) anion. This can be, therefore, looked at as a $(CO)_3Ni \leftarrow L\text{–}L \rightarrow Ni(CO)_3$ carbonyl-substituted pseudo-dinuclear complex of the peculiar $\mathbf{3}^{n-}$ distibine ligand.

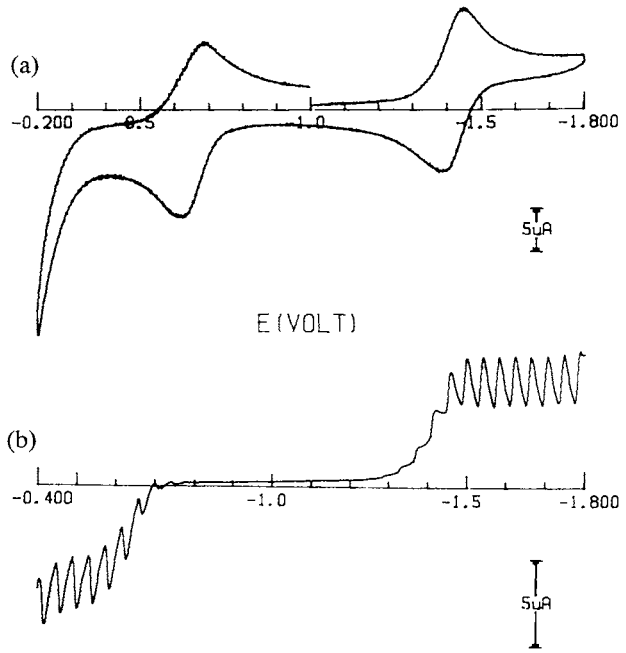

Fig. 1. Voltammetric profiles recorded at a platinum electrode on a MeCN solution containing $\mathbf{3}^{3-}$ (0.7×10^{-3} M) and $[NEt_4][ClO_4]$ (0.1 M). (a) Cyclic voltammogram recorded at 0.2 V s^{-1}. (b) Voltammogram at an electrode with periodical renewal of the diffusion layer recorded at 0.02 V s^{-1}).

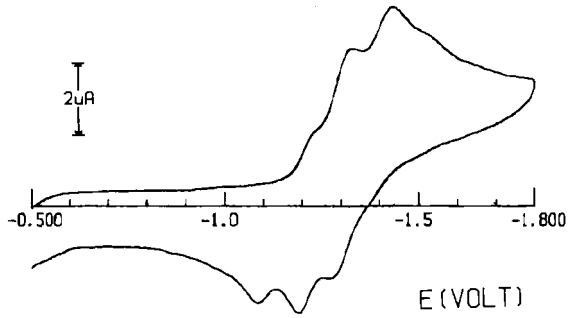

Fig. 2. Cyclic voltammogram recorded at a mercury electrode on a MeCN solution containing $\mathbf{1}^{2-}$ (0.5×10^{-3} M) and $[NEt_4][ClO_4]$ (0.1 M). Scan rate 0.5 V s^{-1}.

2.2. Electrochemical behavior of $\mathbf{1}^{2-}$ and $\mathbf{3}^{3-}$

Fig. 1 shows the profiles exhibited by an acetonitrile solution of $\mathbf{3}^{3-}$ in cyclic voltammetry at a stationary electrode and at an electrode with periodical renewal of the diffusion layer, respectively. The trianion undergoes either an oxidation or a reduction with features of chemical reversibility in the cyclic voltammetry timescale. Controlled potential coulometry in correspondence of the anodic step ($E_w = -0.5$ V) consumes one electron/molecule and the resulting solution displays a voltammetric profile quite complementary to the original one. The formal electrode potentials of the sequence $\mathbf{3}^{2-/3-/4-}$ are compiled in Table 1, together with those of related complexes [10,11].

The isostructural redox sequences $[Ni_{10}E_2(\mu_{12}\text{-}Ni)(CO)_{18}]^{2-/3-/4-}$ (E = Bi, Sb), which occur essentially at the same potential values, are cathodically shifted by about 0.1 V with respect to the corresponding $[Ni_{10}(SbNi(CO)_3)_2(\mu_{12}\text{-}Ni)(CO)_{18}]^{2-/3-/4-}$. Nevertheless, in spite of such electronic effects played by the dangling $Ni(CO)_3$ units present in $\mathbf{2}^{3-}$, no significant difference exists between the HOMO–LUMO gap of $[Ni_{10}E_2(\mu_{12}\text{-}Ni)(CO)_{18}]^{3-}$ (0.76 eV) and that of $\mathbf{2}^{3-}$ (0.72 eV).

As well deducible from the cyclic voltammogram shown in Fig. 2, the $\mathbf{1}^{2-}$ dianion displays a quite different redox aptitude in that it undergoes three subsequent one-electron reductions very close each other. As a matter of fact, controlled potential coulometry in correspondence of the overall process ($E_w = -1.6$ V) consumes rather quickly three electrons/molecule, but the current remains indefinitely somewhat higher than the background current likely because of generation of redox active fragments. Furthermore, cyclic voltammetric tests after electrolysis show ill defined cathodic peaks not due to the original product. Therefore, in spite of features of chemical reversibility of the electron transfer sequence in the cyclic voltammetric timescale, the redox congeners are not stable in the longer times of macroelectrolysis. The formal electrode potentials of the redox changes exhibited by $\mathbf{1}^{2-}$ are summarized in Table 1. A few points connected with the increased nuclearity of this compound with respect to the low-nuclearity species seem worthy of attention: (i) the improvement of its ability to act as an electron sponge; (ii) the remarkable decrease of the HOMO–LUMO gap for the transient trianion $\mathbf{1}^{3-}$ (ca. 0.1 eV); (iii) the

Table 1
Formal electrode potentials (in V, versus SCE) and peak-to-peak separations (in mV) for the redox sequences exhibited by the complexes $\mathbf{3}^{3-}$, $[Ni_{10}Bi_2(\mu_{12}\text{-}Ni)(CO)_{18}]^{3-}$, $\mathbf{2}^{3-}$, and $\mathbf{1}^{2-}$ in acetonitrile solution

Complex	$E^{\circ\prime}_{2-/3-}$	ΔE_p [a]	$E^{\circ\prime}_{3-/4-}$	ΔE_p [a]	$E^{\circ\prime}_{4-/5-}$	ΔE_p [a]	Ref.
$\mathbf{3}^{3-}$	−0.65	74	−1.42	58	–	–	Present work
$[Ni_{10}Bi_2(\mu_{12}\text{-}Ni)(CO)_{18}]^{3-}$	−0.67	70	−1.42	68	–	–	[11]
$\mathbf{2}^{3-}$	−0.56	68	−1.28	66	–	–	[10]
$\mathbf{1}^{2-}$	−1.16	120	−1.25	105	−1.36	130	Present work

[a] Measured at 0.2 V s^{-1}.

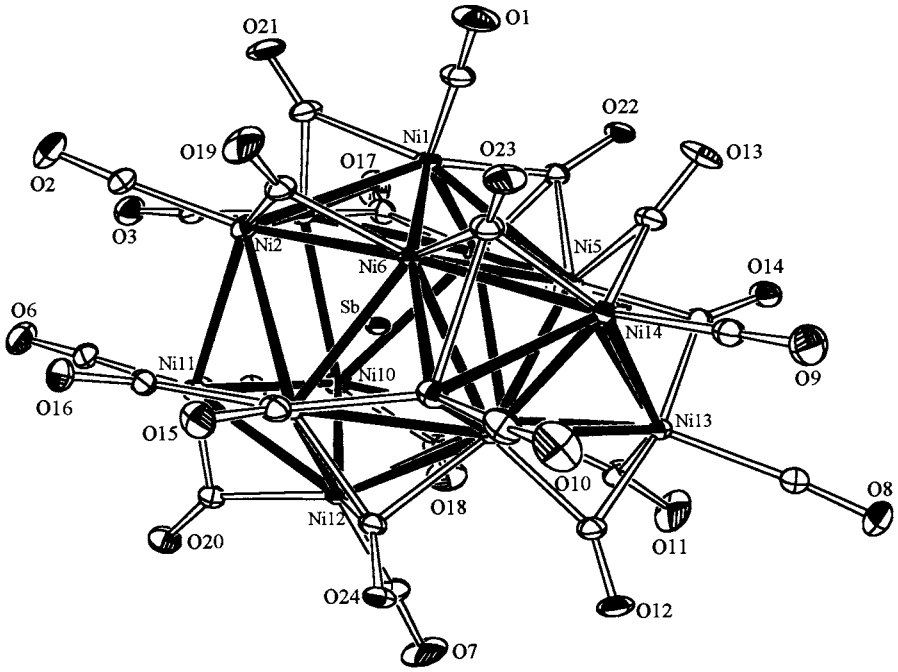

Fig. 3. ORTEP drawing of $\mathbf{1}^{2-}$ (thermal ellipsoids are drawn at 30% probability level).

significant departure of the peak-to-peak separations from the theoretical value of 59 mV, which suggests that the electron transfers induce significant geometrical reorganizations.

2.3. The molecular structures of $[NEt_3CH_2Ph]_2$[1] and $[NEt_4]_3$[3]

The unit cell of $[NEt_3CH_2Ph]_2$[**1**] contains four cluster dianions and eight $[NEt_3CH_2Ph]^+$ cations separated by normal van der Waals interactions. The structure of $\mathbf{1}^{2-}$ (Fig. 3) consists of a very distorted Sb-centered $Ni_{12}(\mu_{12}$-Sb) icosahedral moiety, capped on three adjacent triangular faces by three Ni atoms (Fig. 4). The three capping atoms give rise to a closely packed assembly of metal atoms located on one side of the icosahedron with disruption of the icosahedral symmetry. Only an idealized mirror plane can be envisaged for the metal atom assembly. The Ni–Ni distances (Table 2) of the icosahedral moiety are spread over a wider range with respect to those observed in $[Ni_{12}(\mu_{12}\text{-E})(CO)_{22}]^{2-}$ (E = Sn, Ge), where a more regular icosahedral framework, only slightly elongated along a pseudo C_5 axis is observed [8]. Here some Ni–Ni distances become even larger than 3.00 Å up to the opening of the Ni(3)···Ni(11) edge of the icosahedron which is 3.584(1) Å, a distance out of the range of values usually observed in icosahedral Ni clusters. The average Ni–Sb distance is slightly larger than the average Ni–Sn distance {2.64 Å versus 2.60 Å found in $[Ni_{12}(\mu_{12}$-Sn)$(CO)_{22}]^{2-}$}. The Ni–Ni connectivities range from seven to ten. Apart from the capping Ni(13) and Ni(15) atoms, Ni(2), Ni(3), Ni(10) and Ni(11), belonging to the 'open side' of the icosahedron, are those with lower coordination number (7). The 24 CO ligands are bonded as follows: ten are terminal, eleven edge bridging and three triply bridging. The actual ligand stereogeometry, which is affected by quite high thermal motion, can be considered a frozen image taken out of a fluxional behavior in solution. The distortion of the icosahedral cavity is probably triggered by the size of the encapsulated heteroatom but cannot take place in a symmetric fashion because the walls of the polyhedron are reinforced on one side by the capping atoms. An asymmetric distribution of the ligands and, probably, a

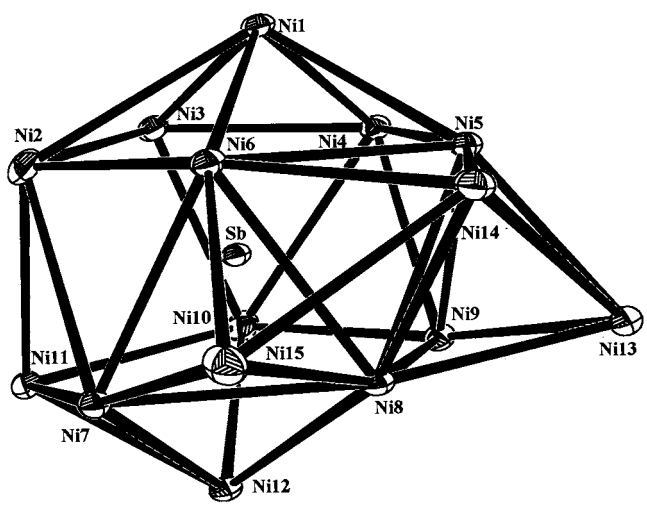

Fig. 4. ORTEP drawing of the $Ni_{15}(\mu_{12}$-Sb) polyhedron.

Table 2
Selected interatomic distances (Å) for $[NEt_3CH_2Ph]_2$[**1**]

Sb–Ni(1)	2.409(1)	Sb–Ni(7)	2.876(1)
Sb–Ni(2)	2.364(1)	Sb–Ni(8)	2.948(1)
Sb–Ni(3)	2.914(1)	Sb–Ni(9)	2.389(1)
Sb–Ni(4)	2.756(1)	Sb–Ni(10)	2.517(1)
Sb–Ni(5)	2.769(1)	Sb–Ni(11)	2.691(1)
Sb–Ni(6)	2.640(1)	Sb–Ni(12)	2.421(1)
Ni(1)–Ni(2)	2.843(1)	Ni(6)–Ni(8)	2.561(1)
Ni(1)–Ni(3)	2.700(1)	Ni(6)–Ni(14)	2.720(1)
Ni(1)–Ni(4)	2.348(1)	Ni(6)–Ni(15)	2.729(1)
Ni(1)–Ni(5)	2.745(1)	Ni(7)–Ni(8)	2.629(1)
Ni(1)–Ni(6)	3.044(1)	Ni(7)–Ni(11)	2.869(1)
Ni(2)–Ni(3)	2.993(1)	Ni(7)–Ni(12)	2.398(1)
Ni(2)–Ni(6)	2.847(1)	Ni(7)–Ni(15)	2.773(1)
Ni(2)–Ni(7)	3.023(1)	Ni(8)–Ni(9)	3.007(1)
Ni(2)–Ni(11)	2.473(1)	Ni(8)–Ni(12)	2.748(1)
Ni(3)–Ni(4)	2.591(1)	Ni(8)–Ni(13)	2.487(1)
Ni(3)–Ni(10)	2.520(1)	Ni(8)–Ni(14)	2.496(1)
Ni(4)–Ni(5)	3.077(1)	Ni(8)–Ni(15)	2.633(1)
Ni(4)–Ni(9)	2.714(1)	Ni(9)–Ni(10)	2.809(1)
Ni(4)–Ni(10)	2.782(1)	Ni(9)–Ni(12)	2.848(1)
Ni(5)–Ni(6)	2.813(1)	Ni(9)–Ni(13)	2.858(1)
Ni(5)–Ni(8)	2.703(1)	Ni(10)–Ni(11)	2.984(1)
Ni(5)–Ni(9)	2.613(1)	Ni(10)–Ni(12)	3.141(1)
Ni(5)–Ni(13)	2.344(1)	Ni(11)–Ni(12)	2.521(1)
Ni(5)–Ni(14)	2.820(1)	Ni(13)–Ni(14)	2.945(1)
Ni(6)–Ni(7)	2.490(1)	Ni(14)–Ni(15)	2.619(1)
Ni–C (terminal)$_{av}$	1.91	CO (terminal)$_{av}$	1.21
Ni–C (double bridg.)$_{av}$	1.95	CO (double bridg.)$_{av}$	1.13
Ni–C (triple bridg.)$_{av}$	2.12	CO (triple bridg.)$_{av}$	1.16

localization of the singly occupied orbital in the vicinity of the open face can do the work (see also Section 3).

Since the initial stages of the refinement, atom Ni(10) showed an unusual thermal displacement parameter, which was quite large if compared to those of the remaining metal atoms, and the same behavior was observed for the carbonyl ligands bound to Ni(10). This apparently higher thermal motion could be explained as deriving from a dynamic behavior of the carbonyl ligands about Ni(10), which in turn can be distributed over different very close positions, thereby simulating a higher displacement parameter. To clarify the situation, a refinement of the occupancy of the Ni(10) site was attempted which resulted in a value of the occupancy close to 0.75 and in an atomic displacement parameter in line with those of all the other nickel atoms. The same refinement was subsequently carried out for the carbonyl ligand bound to Ni(10) which converged approximately to the same value for the occupancy of the sites. This finding can be interpreted in terms of disordered cocrystallization of two anions having different nuclearity, namely $\mathbf{1}^{2-}$ and $[Ni_{14}(\mu_{12}\text{-}Sb)(CO)_{23}]^{2-}$ and in a molar ratio of 3:1. Consequently the latter dianion derives from $\mathbf{1}^{2-}$ by loss of the Ni(10)–C(5)–O(5) fragment and the C(18)–O(18) carbonyl which is a double bridging ligand in $\mathbf{1}^{2-}$, becomes terminal in $[Ni_{14}(\mu_{12}\text{-}Sb)(CO)_{23}]^{2-}$. The two $[NEt_3CH_2Ph]^+$ cations display very similar thermal parameters thus suggesting that full occupation of the cationic sites is achieved. It is not unusual that two clusters having essentially the same steric hindrance are co-crystallized in the same crystal, relevant examples being the recently reported $[Ni_{36}Pt_4(CO)_{45}]^{6-}$–$[Ni_{37}Pt_4(CO)_{46}]^{6-}$ [18] and $Pd_{59}(CO)_{32}(PMe_3)_{21}$–$Pd_{65}(CO)_{26+x}(PMe_3)_{21}$ [19] pair of compounds. As we have not been able to find independent evidence of this model of disorder we keep it as a hypothesis to be proven by further work and we discuss only the 'main molecule' throughout the paper.

The unit cell of $[NEt_4]_3$[**3**] contains four cluster trianions placed around inversion centers, eight cations in general positions and four around twofold axes; therefore the independent part of the structural pattern is half of the formula unit. The molecular structure of $\mathbf{3}^{3-}$ is shown in Fig. 5 and relevant bond lengths and angles are reported in Table 3. The anion contains a centered $Ni_{10}Sb_2(\mu_{12}\text{-}Ni)$ icosahedron with the Sb atoms occupying opposite vertices. The idealized geometry of the metal polyhedron is D_{5d} and it can be alternatively envisaged as a pentagonal antiprism whose pentagonal faces are capped by Sb atoms. Each peripheral Ni atom carries one terminal CO and the eight remaining COs are six doubly bridging the Ni–Ni edges not capped by the antimony atoms and two triply bridging Ni_3 faces. The Sb atoms are devoid of outer ligands as it has been found for the Bi atoms in the isomorphous and isostructural $[Ni_{10}Bi_2(\mu_{12}\text{-}Ni)(CO)_{18}]^{3-}$ [11]. In the previously reported antimony derivatives, namely the Ni-centered $\mathbf{2}^{n-}$ ($n = 2$, 3) [10] and non-centered $[Ni_{10}(\mu_5\text{-}SbPh)_2(CO)_{18}]^{3-}$ [2], two $Ni(CO)_3$ and two phenyl outer ligands coordinate to the two Sb atoms of the icosahedral core, respectively.

The Ni–Ni distances can be divided into three sets: Ni–Ni(intrapentagonal), Ni–Ni(interpentagonal) and Ni(surface)–Ni(interstitial). The Ni–Ni edges of the pentagonal faces (range 2.677–2.846(1) Å, average 2.776 Å) are as expected shorter than those in the analogous $[Ni_{10}Bi_2(\mu_{12}\text{-}Ni)(CO)_{18}]^{3-}$ (average 2.810 Å) because of the smaller size of Sb with respect to Bi and very close to those observed in $\mathbf{2}^{3-}$ (average 2.773 Å). The interpentagonal Ni–Ni distances are the shortest ones (range 2.497–2.529(1) Å, average 2.517 Å) as it has been noted in both $[Ni_{10}Bi_2(\mu_{12}\text{-}Ni)(CO)_{18}]^{3-}$ and $\mathbf{2}^{3-}$ (average 2.518 and 2.506 Å, respectively). The Ni(surface)–Ni(interstitial) interactions (range 2.556–2.598(1) Å, average 2.574 Å) are almost identical to those in $\mathbf{2}^{3-}$ (average 2.578 Å). The icosahedral core is completed by Ni–Sb interactions. The Ni(surface)–Sb bonds fall in the range 2.696–2.725(1) Å (average 2.744 Å) and closely resemble the analogous interaction in $\mathbf{2}^{3-}$ (average 2.748 Å) and finally the Ni(interstitial)–Sb distances are 2.422(1) Å long exhibiting some lengthen-

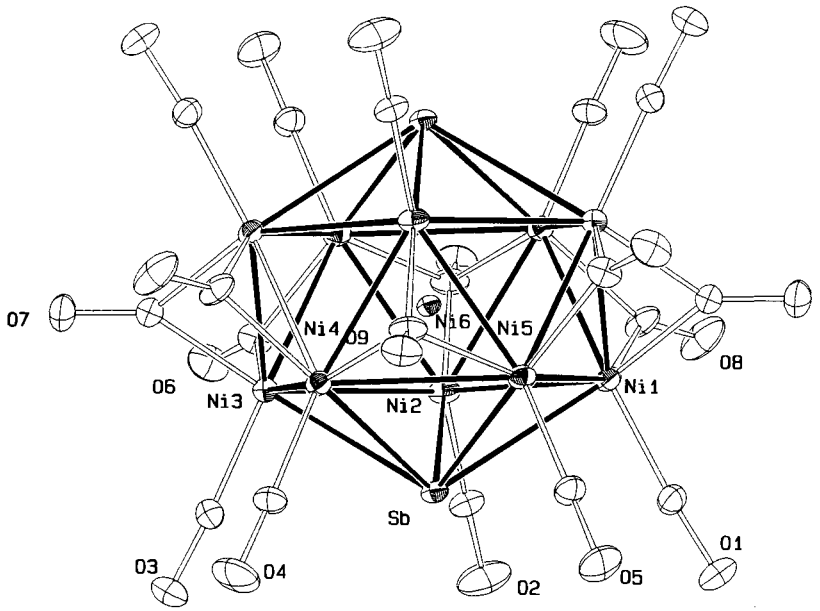

Fig. 5. ORTEP drawing of the $\mathbf{3}^{3-}$ anion (thermal ellipsoids are drawn at 30% of the probability level). The carbon atoms of the carbonyl ligands are labeled in accord with the corresponding oxygens. The anion possesses C_i precise symmetry.

ing in comparison to those in $\mathbf{2}^{3-}$ (2.403(1) Å). In the non-centered $[Ni_{10}(\mu_5\text{-}SbPh)_2(CO)_{18}]^{3-}$ the distance between the two capping Sb atoms along the pseudo fivefold axis averages 3.911 Å [2] indicating a higher compression of the icosahedron in comparison with the two centered $Ni_{10}Sb_2(\mu_{12}\text{-}Ni)$ icosahedra (Sb–Sb′ 4.806 and 4.844(1) Å in $\mathbf{2}^{3-}$ and $\mathbf{2}^{2-}$, respectively).

3. Concluding remarks

We have been so far unable to synthesize a Sb-centered dodecanickel cluster of formula $[Ni_{12}(\mu_{12}\text{-}Sb)(CO)_{22}]^{-}$, isoelectronic with the known $[Ni_{12}(\mu_{12}\text{-}Sn)(CO)_{22}]^{2-}$ [8]. We only succeeded in obtaining a Sb-centered $[Ni_{15}(\mu_{12}\text{-}Sb)(CO)_{24}]^{2-}$ paramagnetic cluster, which is strictly related to the above target compound. This partial failure is probably to ascribe to a combination of steric and electronic effects. Indeed a regular Ni_{12} icosahedral cage appears to be mostly suitable for a third row main group element such as germanium, as shown both by the structure of $[Ni_{12}(\mu_{12}\text{-}Ge)(CO)_{22}]^{2-}$ and the stability under a carbon monoxide atmosphere of the pentagonal antiprismatic $[Ni_{10}(\mu_{10}\text{-}Ge)(CO)_{20}]^{2-}$ [8]. The tin atom is oversized. However, its partial contraction (probably arising from a positive polarization induced by the electronegativity of the $[Ni_{12}(CO)_{22}]^{2-}$ shell) and an elongation along one C_5 axis of the icosahedron are sufficient to permit the existence of $[Ni_{12}(\mu_{12}\text{-}Sn)(CO)_{22}]^{2-}$. The apparent radius of Sn (1.26 Å) in the latter compound is only slightly greater than that displayed by the Ge atom (1.22 Å) in $[Ni_{12}(\mu_{12}\text{-}Ge)(CO)_{22}]^{2-}$. The antimony atom is oversized as Sn. However, it has a higher electronegativity, which probably hinders a sufficiently positive polarization. In $\mathbf{1}^{2-}$ the Sb atom displays an apparent radius of 1.31 Å. The lodging of Sb in an icosahedral Ni cage becomes only possible through distortions of the icosahedral moiety heavier than in the case of the Sn atom. On the other hand, departure from a more regular icosahedral geometry of the above moiety could be eased by the lack of one bonding electron. Indeed, $\mathbf{1}^{2-}$ has 25 skeletal electrons rather than 26 as

Table 3
Selected interatomic distances (Å) for $[NEt_4]_3$[**3**]

Sb–Ni(1)	2.775(1)	Sb–Ni(2)	2.696(1)
Sb–Ni(3)	2.769(1)	Sb–Ni(4)	2.745(1)
Sb–Ni(5)	2.736(1)	Sb–Ni_{av}	2.744
Sb–Ni(interstitial)	2.422(1)		
Ni–$Ni_{intrapentagonal}$			
Ni(1)–Ni(2)	2.774(1)	Ni(2)–Ni(3)	2.746(1)
Ni(3)–Ni(4)	2.839(1)	Ni(4)–Ni(5)	2.677(1)
Ni(1)–Ni(5)	2.846(1)	Ni–$Ni_{intrapentagonal}$(av)	2.776
Ni–$Ni_{interpentagonal}$			
Ni(2)–Ni(4′)	2.509(1)	Ni(2)–Ni(5′)	2.497(1)
Ni(1)–Ni(4′)	2.527(1)	Ni(1)–Ni(3′)	2.527(1)
Ni(3)–Ni(5′)	2.529(1)	Ni–$Ni_{interpentagonal}$(av)	2.517
$Ni_{surface}$–$Ni_{interstitial}$			
Ni(1)–Ni(6)	2.598(1)	Ni(2)–Ni(6)	2.556(1)
Ni(3)–Ni(6)	2.587(1)	Ni(4)–Ni(6)	2.567(1)
Ni(5)–Ni(6)	2.563(1)	$Ni_{surface}$–$Ni_{interstitial}$	2.574
Ni–C (terminal)$_{av}$	1.76	CO (terminal)$_{av}$	1.13
Ni–C (double bridg.)$_{av}$	1.90	CO (double bridg.)$_{av}$	1.16
Ni–C (triple bridg.)$_{av}$	2.04	CO (triple bridg.)	1.183(6)

$[Ni_{12}(\mu_{12}\text{-}Sn)(CO)_{22}]^{2-}$. This interpretation mirrors the previously reported rationalization of the paramagnetic $[Co_6(\mu_6\text{-}C)(CO)_{14}]^{-}$ octahedral cluster, whose stability was suggested to arise from synergy between steric pressure exerted by the interstitial carbon atom and localized weakening of one Co–Co interaction produced by the presence of an antibonding electron [20]. The above rationalization of $\mathbf{1}^{2-}$ is partially supported by its redox and chemical behavior. Indeed, although it undergoes quasi-reversible reductions, the electrogenerated species are only stable on the cyclic voltammetric timescale. Furthermore, the compound is readily degraded by carbon monoxide and is eventually converted in the most stable Ni-centered $\mathbf{3}^{n-}$ and $\mathbf{2}^{n-}$ derivatives. The above conversion apparently derives from condensation of two labile $[Ni_6Sb(CO)_x]^{2-}$ molecules arising by disproportionation of $\mathbf{1}^{2-}$ under a carbon monoxide atmosphere. A related condensation originating from disproportionation induced by PPh_3 has previously allowed to obtain $[Ni_{16}(C_2)_2(CO)_{23}]^{4-}$ from $[Ni_{10}C_2(CO)_{16}]^{2-}$ [21].

According to previous EHMO calculations [10] suggesting that lodging of a late transition metal in an icosahedral Ni_{12} or $Ni_{10}E_2$ cage could alter the number of SEPs, the $\mathbf{3}^{n-}$ ($n = 2$, 3, 4) cluster displays 17–18 filled cluster valence orbitals (depending on the value of n) rather than 13. The stability of $\mathbf{3}^{n-}$ in three different oxidation states is probably due to the non-bonding nature of its frontier orbitals and the probable strengthening of the metal framework imparted by the interstitial nickel and the peripheral antimony atoms.

4. Experimental

All reactions including sample manipulations were carried out using standard Schlenk techniques under nitrogen and in carefully dried solvents. The $[Ni_6(CO)_{12}]^{2-}$ and $\mathbf{2}^{3-}$ salts have been prepared according to the literature [10,22]. Analyses of Ni were performed by atomic absorption on a Pye-Unicam instrument. IR spectra were recorded on a Perkin Elmer 1605 interferometer using CaF_2 cells. EPR spectra have been recorded on a Bruker ESP 300E spectrometer and magnetic moments have been measured with a Sherwood magnetic balance. Material and apparatus for electrochemistry have been described elsewhere [23]. Voltammetry at electrodes with periodical renewal of diffusion layer were performed according to literature [24]. All potential values are referred to the saturated calomel electrode (SCE). Under the present experimental conditions the one electron oxidation of ferrocene occurs at $E^{\circ\prime} = +0.38$ V.

4.1. Synthesis of $[NEt_4]_2$[1]

$[NEt_4]_2[Ni_6(CO)_{12}]$ (5.08 g, 5.36 mmol) was dissolved in anhydrous acetonitrile (50 ml) in a 250 ml flask under a nitrogen atmosphere. A solution of $SbCl_3$ (0.49 g, 2.14 mmol) in anhydrous acetonitrile (30 ml) was added in portions under stirring over a period of two hours, while continually removing the developing carbon monoxide with a slow stream of nitrogen. The resulting brown suspension was evaporated to dryness under vacuum. The residue was washed with water (30 ml), THF (20 ml) and methanol (30 ml), and extracted with acetone (50 ml). The acetone solution was concentrated to ca. 30 ml and precipitated by diffusion of isopropyl alcohol (50 ml) to give 2.31 g of $[NEt_4]_2$[**1**] as black crystals. Anal. Found: C, 25.15; H, 2.21; N, 1.47; Ni, 45.12. Calc. for $[NEt_4]_2$[**1**]: C, 24.81; H, 2.07; N, 1.45; Ni, 45.52%.

4.2. Synthesis of $[NEt_3CH_2Ph]_2$[1]

Solid $[NEt_4]_2$[**1**] (1.86 g) was dissolved in acetonitrile (30 ml) and a solution of $[NEt_3CH_2Ph]Cl$ (2.73 g) in water (20 ml) was dropwise added under vigorous stirring. The resulting brown precipitate was filtered, was washed with water (50 ml in portions) and methanol (20 ml) and dried in vacuo. Extraction of the precipitate with acetone (30 ml) and precipitation by diffusion of isopropyl alcohol (70 ml) gave 1.76 g of $[NEt_3CH_2Ph]_2$[**1**] as black crystals. Anal. Found: C, 29.33; H, 2.26; N, 1.27; Ni, 42.50. Calc. for $[NEt_3CH_2Ph]_2$[**1**]: C, 29.15; H, 2.14; N, 1.36; Ni, 42.78%.

4.3. Synthesis of $[NEt_4]_3$[3]

Solid $[NEt_4]_3$[**2**] (1.21 g, 0.58 mmol) was dissolved in acetone (30 ml) and solid PPh_3 (0.31 g, 1.18 mmol) was added in portions under stirring. The resulting brown mixture was evaporated to dryness and the residue was suspended in toluene (30 ml) and filtered. After several washings in THF, the residue was extracted in acetone (30 ml) and precipitated by diffusion of isopropyl alcohol (50 ml) to give 0.74 g of $[NEt_4]_3$[**3**] as black crystals. Anal. Found: C, 28.05; H, 3.43; N, 2.28; Ni, 36.31. Calc. for $[NEt_4]_3$[**3**]: C, 28.26; H, 3.36; N, 2.36; Ni, 36.21%.

4.4. X-ray data collection and structure determination of $[NEt_3CH_2Ph]_2$[1] and $[NEt_4]_3$[3]

4.4.1. $[NEt_3CH_2Ph]_2$[1]

A crystal sample of dimensions $0.12 \times 0.14 \times 0.20$ mm was mounted on a glass fiber in air and collected at room temperature on a Siemens SMART CCD area-detector diffractometer. Crystal data are reported in

Table 4
Crystallographic data for $[NEt_3CH_2Ph]_2$[**1**] and $[NEt_4]_3$[**3**]

Compound	$[NEt_3CH_2Ph]_2$[**1**]	$[NEt_4]_3$[**3**]
Formula weight (amu)	2030.59	1784.24
Crystal system	Monoclinic	Orthorhombic
a (Å)	19.269(2)	21.132(6)
b (Å)	15.098(1)	19.622(6)
c (Å)	22.688(1)	14.444(5)
β (°)	92.87(1)	90
V (Å^3)	6592.2(9)	5989(3)
Space group	$P2_1/c$ (no. 14)	$Pccn$ (no. 56)
Z	4	4
μ(Mo–K$_\alpha$) (cm^{-1})	45.77	43.19
Unique reflections	15 065 ($\pm h$, $\pm k$, $\pm l$)	7173 ($+h$, $+k$, $+l$)
Observed reflections [$I>2\sigma(I)$]	10577	5047
Final R and R_w indices [a]	0.035, 0.092	0.035, 0.093

[a] $R=[\Sigma||F_o|-|F_c||/\Sigma|F_o|]$; $R_w=[\Sigma w(F_o-F_c)^2/\Sigma wF_o^2]^{0.5}$.

Table 4. Graphite-monochromatized Mo–K$_\alpha$ ($\lambda=0.71073$ Å) radiation was used with the generator working at 50 kV and 35 mA. Cell parameters and orientation matrix were obtained from least-squares refinement on 315 reflections measured in three different sets of 15 frames each, in the range $0<\theta<23°$. The intensity data were collected within the limits $8<2\theta<56.6°$ in the full sphere (scan method), with sample-detector distance fixed at 5 cm. A total of 2100 frames (20 s per frame; $\Delta\omega=0.3°$) were collected; the first 100 frames, were recollected to have a monitoring of crystal decay, which was not observed; an absorption correction was applied (SADABS [25]). A total of 73033 reflections were collected (15609 unique, $R_{int}=0.025$; $R_\sigma=0.062$ [26]). The structure was solved by direct methods (SIR-97) [27] and refined with full-matrix-block least-squares (SHELX-97) [28] on the basis of 9615 independent reflections with $I>2\sigma(I)$; anisotropic temperature factors were assigned to all non-hydrogen atoms. Hydrogens of the cations were riding on their carbon atoms.

4.4.2. $[NEt_4]_3$[3]

Crystal data and other experimental details are reported in Table 4. A crystal with dimensions of $0.15\times0.23\times0.35$ mm was mounted on tip of a glass fiber. The diffraction experiments were carried out on an Enraf–Nonius CAD4 diffractometer at 223 K, using graphite-monochromatized Mo–K$_\alpha$ radiation ($\lambda=0.71073$ Å). The unit cell was determined by a least-squares fitting procedure using 25 randomly selected strong reflections. The diffracted intensities were corrected for Lorentz, polarization and absorption (empirical correction). The metal atom positions were determined by direct methods (SIR-97 [27]) and all non-hydrogen atoms located from Fourier difference syntheses. Hydrogen atoms were added in calculated positions (d_{C-H} 0.98 Å). The final refinement on F^2 proceeded by full-matrix least-squares calculations (SHELX-97 [28]) using anisotropic thermal parameters for all the non-hydrogen atoms. The methyl and methylene hydrogen atoms were assigned an isotropic thermal parameters 1.5 times the U_{eq} values of the carrier carbon atoms.

5. Supplementary material

Crystallographic data for the structural analysis have been deposited with the Cambridge Crystallographic Data Centre, CCDC no. 125663 for $[NEt_3CH_2Ph]_2$[**1**] and 125664 for $[NEt_4]_3$[**3**].

Acknowledgements

We thank the University of Bologna and the MURST (Cofin98) for a grant and Dr. S. Strazzari for the EPR measurements.

References

[1] D.F. Rieck, R.A. Montag, T.S. McKechnie, L.F. Dahl, J. Am. Chem. Soc. 108 (1986) 1330.
[2] R.E. Des Enfants, J.A. Gavney, R.K. Hayashi, A.D. Rae, L.F. Dahl, J. Organomet. Chem. 383 (1990) 543.
[3] D.F. Rieck, J.A. Gavney, R.L. Norman, R.K. Hayashi, L.F. Dahl, J. Am. Chem. Soc. 114 (1992) 10369.
[4] P.D. Mlynek, L.F. Dahl, Organometallics 16 (1997) 1656.
[5] P.D. Mlynek, L.F. Dahl, Organometallics 16 (1997) 1641.
[6] A.J. Kahaian, J.B. Thoden, L.F. Dahl, J. Chem. Soc. Chem. Commun. (1992) 353.
[7] J.P. Zebrowski, R.K. Hayashi, L.F. Dahl, J. Am. Chem. Soc. 115 (1993) 1142.
[8] A. Ceriotti, F. Demartin, B.T. Heaton, P. Ingallina, G. Longoni, M. Manassero, M. Marchionna, N. Masciocchi, J. Chem. Soc. Chem. Commun. (1989) 786.
[9] V.G. Albano, F. Demartin, M.C. Iapalucci, G. Longoni, A. Sironi, V. Zanotti, J. Chem. Soc. Chem. Commun. (1990) 547.
[10] V.G. Albano, F. Demartin, M.C. Iapalucci, F. Laschi, G. Longoni, A. Sironi, P. Zanello, J. Chem. Soc. Dalton Trans. (1991) 739.
[11] D.M.P. Mingos, T. Slee, L. Zhenyang, Chem. Rev. 90 (1990) 383.
[12] V.G. Albano, F. Demartin, M.C. Iapalucci, G. Longoni, M. Monari, P. Zanello, J. Chem. Soc. Dalton Trans. (1992) 497.
[13] P. Lemoine, Coord. Chem. Rev. 47 (1982) 55.
[14] P. Lemoine, Coord. Chem. Rev. 83 (1988) 169.
[15] P. Zanello, in: P. Zanello (Ed.), Stereochemistry of Organometallic and Inorganic Compounds, vol. 5, Elsevier, Amsterdam, 1994, p. 163.
[16] P. Zanello, Structure and Bonding, Spinger-Verlag, Berlin, 79 (1992) 101.
[17] G. Longoni, C. Femoni, M.C. Iapalucci, P. Zanello, in: P. Braunstein, L. Oro, P. Raithby (Eds.), Metal Clusters in Chemistry, vol. II, Wiley–VCH, Weinheim, 1999, p. 1137.
[18] F. Demartin, C. Femoni, M.C. Iapalucci, G. Longoni, P. Macchi, Angew. Chem. Int. Ed. Engl. 38 (1999) 531.

[19] N.T. Tran, M. Kawano, D.R. Powell, L.F. Dahl, J. Am. Chem. Soc. 120 (1998) 10986.
[20] V.G. Albano, P. Chini, G. Ciani, M. Sansoni, S. Martinengo, J. Chem. Soc. Dalton Trans. (1980) 163.
[21] A. Ceriotti, G. Longoni, M. Manassero, N. Masciocchi, G. Piro, L. Resconi, M. Sansoni, J. Chem. Soc. Chem. Commun. (1985) 1402.
[22] A. Ceriotti, G. Longoni, G. Piva, Inorg. Synth. 26 (1989) 312.
[23] D. Osella, M. Ravera, C. Nervi, C.E. Housecroft, P.R. Raithby, P. Zanello, F. Laschi, Organometallics 10 (1991) 3253.
[24] G. Schiavon, G.A. Mazzocchin, G.G. Bombi, J. Electroanal. Chem. 9 (1971) 401.
[25] G.M. Sheldrick, SADABS, University of Göttingen, Germany, 1996.
[26] $R_{\text{int}} = \Sigma|F_o^2 - F_{\text{mean}}^2|/\Sigma F_o^2$; $R_\sigma = \Sigma\sigma(F_o^2)/\Sigma F_o^2$.
[27] A. Altomare, G. Cascarano, C. Giacovazzo, A. Guagliardi, A.G.G. Moliterni, M.C. Burla, G. Polidori, M. Camalli, R. Spagna, SIR-97, A Package for Crystal Structure Solution by Direct Methods and Refinement, University of Bari, Italy, 1997.
[28] G.M. Sheldrick, SHELXL-97, Program for the Refinement of Crystal Structures, University of Göttingen, Germany, 1997.